Journal of
Marine Science and Engineering

MDPI

Article

Experimental Validation of Smoothed Particle Hydrodynamics on Generation and Propagation of Water Waves

Andi Trimulyono [1,2,*] and Hirotada Hashimoto [1]

[1] Graduate School of Maritime Sciences, Kobe University, Kobe 658-0022, Japan; hashimoto@port.kobe-u.ac.jp
[2] Department of Naval Architecture, Diponegoro University, Semarang 50275, Indonesia
* Correspondence: anditrimulyono@gmail.com; Tel.: +81-8025-295-499

Received: 22 November 2018; Accepted: 14 January 2019; Published: 18 January 2019

Abstract: This paper is aimed to validate smoothed particle hydrodynamics (SPH) on the generation and propagation of water waves. It is a classical problem in marine engineering but a still important problem because there is a strong demand to generate intended nonlinear water waves and to predict complicated interactions between nonlinear water waves and fixed/floating bodies, which is indispensable for further ocean utilization and development. A dedicated experiment was conducted in a large wave basin of Kobe University equipped with a piston-type wavemaker, at three water depths using several amplitudes and periods of piston motion for the validation of SPH mainly on the long-distance propagation of water waves. An SPH-based two-dimensional numerical wave tank (NWT) is used for numerical simulation and is accelerated by a graphics processing units (GPU), assuming future applications to realistic engineering problems. In addition, comparison of large-deformation of shallow water waves, when passing over a fixed box-shape obstacle, is also investigated to discuss the applicability to wave-structure interaction problems. Finally, an SPH-based three-dimensional NWT is also validated by comparing with an experiment and two-dimensional simulation. Through these validation studies, detailed discussion on the accuracy of SPH simulation of water waves is made as well as providing a recommended set of SPH parameters.

Keywords: SPH; Experimental validation; Water waves; Numerical wave tank; GPU

1. Introduction

Generation and propagation of water waves is a classical problem in marine engineering and coastal engineering. One of the difficulties of water wave problems is to handle wave nonlinearities and large deformations of sea-surface. There have been a lot of theoretical, experimental and numerical studies on this issue. In recent years, numerical methods have shown prominent progress among them along with the rapid development of computer performance. Especially general purpose computing on graphics processing units (GPGPU) is one of the key technologies in computer science/engineering to drastically accelerate the computation speed. By introducing the GPGPU technology, computational fluid dynamics (CFD) can be more viable and reliable solution compared to ordinary CFD computation running on central processing units (CPU).

Among CFD methods, so-called particle method has advantages to handle nonlinear free-surface flows and complicated interactions with fixed/floating bodies. One of the well-developed particle methods is smoothed particle hydrodynamics (SPH) that was originally developed for astrophysics [1,2] and it was first applied to free-surface flow problems by Monaghan [3]. Since SPH is a mesh-less and Lagrangian method, special treatment is not required to track the free-surface while a lot of numerical difficulties and problems need to be solved in mesh-based CFDs. Therefore the

particle method including SPH has been applied to violent flows or large deformation of free-surface, such as green water [4,5], sloshing [6,7], fluid-structure interactions [8,9]. SPH simulation of water wave propagation was demonstrated by Violeau and Rogers [10] as a new free-surface capturing method compared to other methods such as volume of fluid (VOF) or level set (LS). SPH has been adopted also in coastal engineering. Dalrymple and Rogers [11] showed that SPH using different time step algorithm is able to model the breaking waves onto beaches both in two- and three-dimensions. Recent studies [12–14] applied SPH to the problem of wave propagation and showed good accuracy, but discussions were made only for short propagation-distance.

Altomare et al. [15] showed SPH verification for medium propagation-distance, in which SPH simulation was compared with the second-order Stokes theory and concluded that SPH is comparable with high-order wave theory even for medium propagation-distance. As the next step, it is expected to validate SPH simulation of water waves in long propagation-distance with systematic comparisons with experimental data measured at a large wave tank. This is important for SPH development/utilization because SPH simulation, adopting fully explicit time-marching, can be drastically accelerated by GPGPU technology so that much larger NWTs can be available in the near future. In the present paper, an open source GPGPU SPH solver, DualSPHysics [16] is used for realizing a large NWT and for validation of SPH on the wave long propagation. GPGPU technology is implemented in DualSPHysics by Crespo et al. [17].

For the validation of SPH on generation and propagation of water waves in a large NWT, a dedicated experiment was conducted at a 60 m wave basin at Kobe University that equipped with a piston-type wavemaker. For the comprehensive validation, the experiment was conducted for three water depths covering deep to shallow water waves, and three amplitudes and two periods of piston motion of wave-making board and the wave elevation and wave pressure at a point far from the wavemaker were measured. For realizing quantitative validation, all SPH simulations were executed by directly imposing the piston motion of wave-making board measured in the experiment, as a moving-wall boundary condition (BC). In order to discuss the validity of SPH on large-deformation of wave surface, the profile of a wave surface when passing a box-shape obstacle set on the water bottom was also measured by a video camera. The comparisons between two-dimensional SPH simulation and the wave tank test demonstrated that the SPH simulation well reproduces the generation, propagation, and deformation of water waves even for the large NWT. Finally, three-dimensional SPH simulation is also performed to confirm the validity as well as two-dimensional SPH because three-dimensional effects need to be dealt with in most engineering applications. Because DualSPHysics version 4.0 has not yet been implemented in multi-GPU parallelization, it made computation cost in three-dimensional NWT is very high. Computation time will reduce when it has been implemented with multi-GPU using message passage interface (MPI) as Dominguez et al. [18] and Hashimoto et al. [9]. Through the comprehensive validations, the validity and the accuracy of SPH on generation and propagation of water waves in a large NWT are discussed with providing appropriate sets of input parameters for SPH.

2. SPH

SPH was initially developed for an astrophysical problem and it has been widely used in marine engineering since the first application to a free-surface flow by Monaghan [3]. SPH is a meshless and Lagrangian method that uses interpolation scheme to approximate physical values and derivatives of continuous field by using discrete evaluation points. The evaluation points are identified as smoothed particles that contain mass, velocity, and position. The quantities are obtained as a weighted average from adjacent particles within the smoothing length, h, to reduce the range of contribution from the neighbor particles. The main features of the SPH method, which is based on integral interpolants,

are described in detail in [19,20]. In SPH, the field function $F(\boldsymbol{r})$ in domain Ω can be approximated by integral approximation as Equation (1) where W is kernel function and $\boldsymbol{r}$ is a vector of position.

$$F(\boldsymbol{r}) = \int_{\Omega} F(\boldsymbol{r}')W(\boldsymbol{r}-\boldsymbol{r}', h)d\boldsymbol{r}' \tag{1}$$

The equation (1) can be approximated into a discrete form by replacing the integral with a summation over the neighboring particles in the compact support of particle a at the spatial position $\boldsymbol{r}$, thus leading to particle approximation of equation (1) becomes

$$F(\boldsymbol{r}_a) \approx \sum_b F(\boldsymbol{r}_b)W(\boldsymbol{r}_a-\boldsymbol{r}_b, h)\frac{m_b}{\rho_b} \tag{2}$$

where the volume associated with neighboring particle b is m_b/ρ_b with m, ρ are mass and density. In this paper, Wendland kernel [21] is used and is shown by Equation (3)

$$W(q) = \alpha_D\left(1-\frac{q}{2}\right)^4(2q+1) \quad 0 \le q \le 2 \tag{3}$$

where α_D is equal to $7/4\pi h^2$ in 2-D and $21/164\pi h^3$ in 3-D. q is the non-dimensional distance between particles a and b that is given r/h. The momentum equation to be solved in SPH is shown in Equation (4).

$$\begin{aligned} \frac{d\boldsymbol{v}_a}{dt} &= -\sum_b m_b\left(\frac{P_{a+P_b}}{\rho_a\cdot\rho_b}+\Pi_{ab}\right)\nabla_a W_{ab} + g \\ \text{Where } \Pi_{ab} &= \begin{cases} \frac{-\alpha\overline{c_{ab}}\mu_{ab}}{\overline{\rho_{ab}}} & \boldsymbol{v}_{ab}\cdot\boldsymbol{r}_{ab} < 0 \\ 0 & \boldsymbol{v}_{ab}\cdot\boldsymbol{r}_{ab} > 0 \end{cases} \end{aligned} \tag{4}$$

where g is gravity acceleration, P_a and P_b are pressure in particle a and b. Π_{ab} is the artificial viscosity term according to Monaghan [22] is used on this paper. Where $\mu_{ab} = h\boldsymbol{v}_{ab}\cdot\frac{\boldsymbol{r}_{ab}}{(r_{ab}^2+\eta^2)}$; $\boldsymbol{r}_{ab} = \boldsymbol{r}_a - \boldsymbol{r}_b$; $\boldsymbol{v}_{ab} = \boldsymbol{v}_a - \boldsymbol{v}_b$ with $\boldsymbol{r}$ and $\boldsymbol{v}$ are vector position and vector velocity. Where $\overline{c_{ab}} = 0.5(c_a + c_b)$ is the mean speed of sound and $\eta^2 = 0.01h^2$ with α is a coefficient that needs to be tuned to get proper dissipation. In this paper we use α = 0.0001 and 0.01.

The continuity equation for basic SPH is shown in Equation (5). The additional term of delta-SPH (δ) based on Molteni and Colagrossi [23]; Marrone et al. [24] is introduced to suppress the density fluctuation, so the equation of continuity becomes Equation (6). In this paper delta-SPH coefficient 0.1 is used in all numerical simulation.

$$\frac{d\rho_a}{dt} = \sum_b m_b(\boldsymbol{v}_a - \boldsymbol{v}_b)\nabla_a W_{ab} \tag{5}$$

$$\frac{d\rho_a}{dt} = \sum_b m_b\boldsymbol{v}_{ab}\cdot\nabla_a W_{ab} + 2\delta h c_0\sum_b(\rho_{b-}\rho_a)\frac{\boldsymbol{r}_{ab}\cdot\nabla_a W_{ab}}{\boldsymbol{r}_{ab}^2}\frac{m_b}{\rho_b} \tag{6}$$

DualSPHysics is based on weakly compressible smoothed particle hydrodynamics (WCSPH) in WCSPH, the fluid is treated as weakly compressible, and hence a state equation given by Equation (7) is used to determine the pressure field based on the computed particle density, where $b = \frac{c_0^2\rho_0}{\gamma}$, $c_0 = c(\rho_0) = \left.\frac{\sqrt{\partial P}}{\partial\rho}\right|_{\rho 0}$, γ = 7; with c_o, ρ_0 and γ are the speed of sound at reference density, the reference density and, respectively, the polytrophic constant.

$$P = b\left[\left(\frac{\rho}{\rho_0}\right)^{\gamma} - 1\right] \tag{7}$$

3. Experimental Condition

A dedicated experiment for the validation of SPH was conducted at a large wave basin of Kobe University, with the dimension of 60 m length, 6 m width and 0 to 1.5 m changeable water depth. The wave basin is equipped with a piston-type wavemaker that can generate both regular and irregular waves. Prior to the experiment, a wave generation trial is repeated for three water depths, those are 0.4 m, 0.75 m and 1.1 m, to find input gains that can realize the same amplitudes of the piston motion for all three water depths. The experiment was conducted as illustrated in the following. Firstly regular waves were generated for each water depth and the wave elevation at 24.6 m distance from the front face of the wave-making board was measured by a wave probe. The time-variation of wave pressure was also measured by a pressure gauge set on the bottom of the basin at the same distance as the wave probe (see Figure 1). The positions of wave probe and pressure gauge were far enough from the wavemaker so that the validity of SPH on the long-distance propagation of water waves can be discussed. In the experiment, regular waves were generated using three piston amplitudes of the wave-making board, which were 16.5 mm, 33.0 mm and 50.5 mm. Two periods of piston motion of 1.95 s and 1.15 s were used. The piston motion of the wave-making board was measured by a laser sensor Keyence IL-600 (Keyence, Osaka, Japan) (see Figure 2) and the measured time histories of the piston motion are shown in Figure 3. These time histories do not depend on the water depth and will be directly used for SPH simulation as input motions. Figure 4 shows measured wave elevation in three water depths for period of 1.15 s with amplitude 50.5 mm. Figure 5 shows measured pressure at the bottom tank for period of 1.95 s with amplitude of wavemaker 50.5 mm. Figure 6 shows the experiment set up for capture large deformations of wave surface using box-shape obstacle. Wave probe is put in the middle of the obstacle to capture the wave elevation of free-surface. The water depths were decided to cover deep water waves to shallow water waves for two wave periods. The ratio of water depth (d) to wavelength (λ) is presented in Table 1 and the combination of water depth of 1.1 m and period of 1.15 s represents the deep water waves, and the others are shallow water waves. Here the wavelength is calculated by Equation (8) which is the theoretical solution under the assumption of small wave amplitude [25]. Table 2 shows the calculated Froude number for a combination of different water depths and periods of wavemaker. Froude number is calculated with Equation (9) where d is depth, U is celerity. It shows the period of 1.15 s is subcritical flow on the other hand the period of 1.95 s is a combination of supercritical and subcritical flow.

$$\lambda = \frac{gT^2}{2\pi} tanh\left(\frac{2\pi d}{\lambda}\right) \tag{8}$$

$$Fn = \frac{U}{\sqrt{gd}} \tag{9}$$

Table 1. Water depths, the ratio between depths and wavelength.

Water Depth	T = 1.95 (s)	T = 1.15 (s)
	(d/λ)	
1.10	0.21	0.53
0.75	0.16	0.37
0.40	0.11	0.22

Table 2. Froude number in three water depths.

Water Depth	T = 1.95 (s)	T = 1.15 (s)
	Fn	
1.10	0.93	0.55
0.75	1.12	0.66
0.40	1.54	0.91

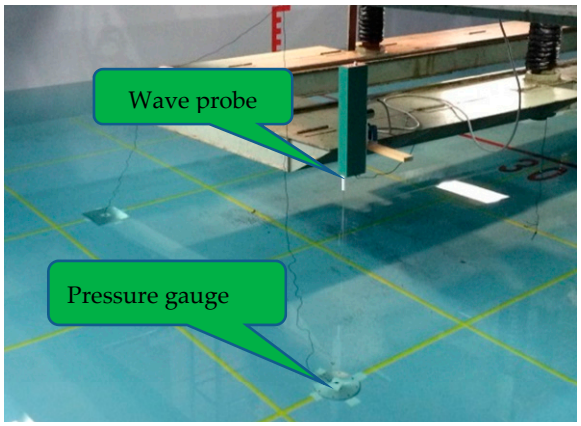

Figure 1. Wave probe and pressure sensor set at 24.6 m from wavemaker.

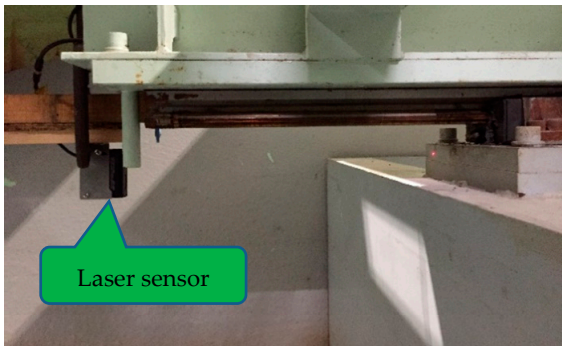

Figure 2. Laser sensor attached to the base frame to measure piston motion.

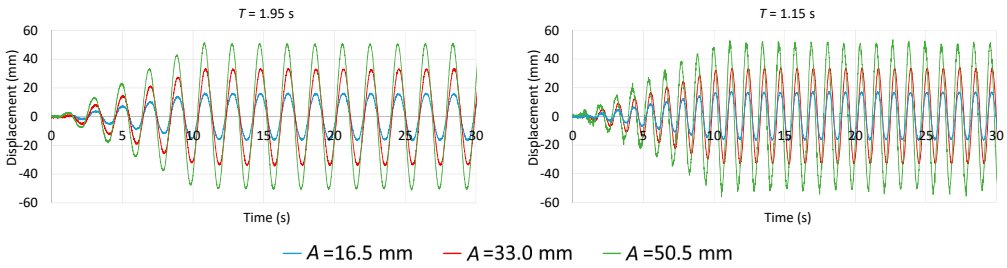

Figure 3. Measured piston motions of wave-making board.

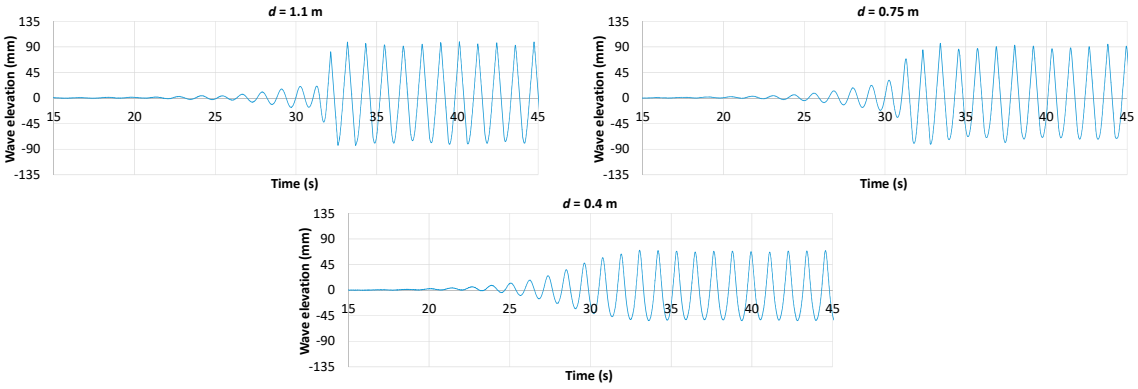

Figure 4. Measured wave elevation on three water depths with T = 1.15 s and A = 50.5 mm.

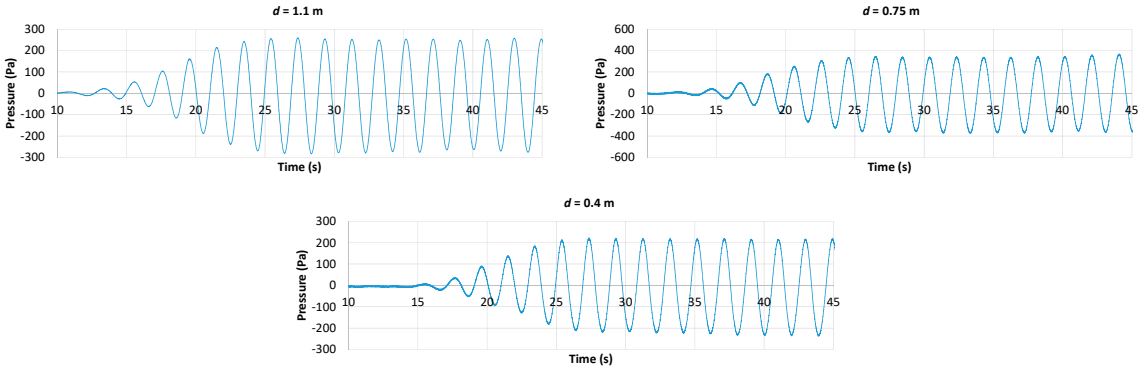

Figure 5. Measured pressure on three water depths with T = 1.95 s and A = 50.5 mm.

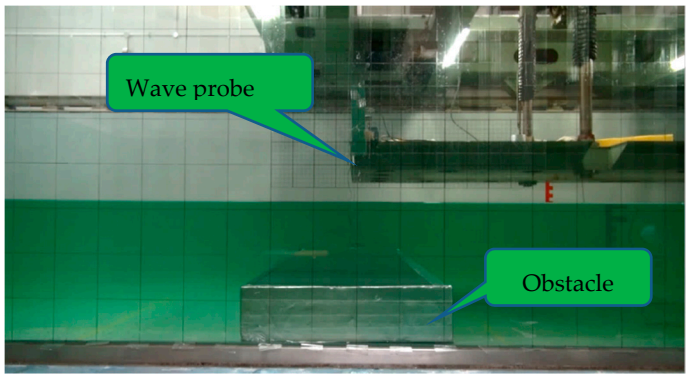

Figure 6. Experimental setup with a box-shape obstacle.

4. Numerical Condition

To reproduce the observed water waves in the experiment, a NWT with the same dimension of the wave basin used in the experiment was prepared. The schematic view of the NWTs with and without the obstacle box is shown in Figure 7. The wave probe, the pressure sensor, and the obstacle box are also put at the same positions as the experiment. Here two-dimensional SPH simulation was executed because single directional regular waves were generated in the experiment. The parameters used in DualSPHysics were set as shown in Table 3. Here "coefh" is defined as $h/dp\sqrt{2}$ where dp means the particle spacing. Artificial viscosity coefficient, α, needs to be tuned to get proper dissipation in water wave propagation problem. After a systematic trial, the optimal value of α was determined to 0.0001 for the subject problem, while α of 0.01 was recommended to use to get proper dissipation in a smaller NWT. Coefsound is defined $Cs/\sqrt{g.d_{swl}}$ where Cs and d_{swl} are the speed of sound, respectively, and the height of water in rest condition. CFL number is a coefficient to calculate time step to satisfy Courant-Friedrichs-Lewy condition. The constant particle spacing of 3.0 mm is used for SPH simulations throughout the paper. The particle spacing was determined through a grid study and its result is presented in the following section. The total number of particles for three water depths is shown in Table 4. In SPH simulation, wave generation was executed by directly imposing the measured piston motion of wavemaker as a moving wall BC without any tuning of the piston stroke. This is an important point to discuss the correctness of physics simulated by the SPH model.

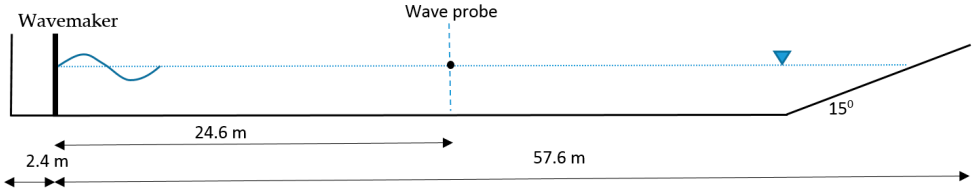

Figure 7. *Cont.*

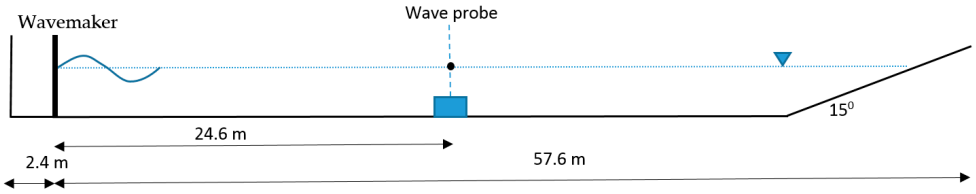

Figure 7. Experimental setup with and without obstacle.

Table 3. Numerical setting in DualSPHysics.

Kernel function	Wendland
Time step algorithm	Symplectic
Artificial viscosity coeff. α	0.0001
Coefsound	20.0
Particle spacing (mm)	3.0
Coefh	2.0
CFL number	0.3
Delta-SPH (δ)	0.1
Simulation time (s)	45.0

Table 4. Total number of particles for three water depths.

Particle Spacing *dp* (mm)	Water Depth *d* (m)	Total Number of Particles
3.0	1.10	6,724,154
	0.75	4,521,922
	0.40	2,338,834

5. Results and Discussion

5.1. Generation and Propagation of Water Waves

SPH simulation was performed using an NVIDIA Titan X 12GB GDDR5. Computation time for the deepest water depth, i.e. 1.1 m, is about 65 h for 50 s simulation including 5 s stationary time for settling down the fluid particles before imposing the wave-maker movement. Firstly a grid study using several particle spacing 2.0 mm, 3.0 mm, 4.0 mm, 5.0 mm and 6.0 mm, was done to investigate the sensitivity of the numerical result to the particle spacing. Table 5 shows total number of particles for grid study for water depth 0.4 m. Figure 8 shows the result of grid study for the smallest water depth of 0.4 m with the minimum piston stroke of 16.5 mm. It shows that the evolution of wave elevation is sensitivity to particle spacing (*dp*). Particle spacing 2.0 mm and 3.0 mm show similar results, but to get reasonable accuracy and computation time, particle spacing 3.0 mm is more favorable to use compared to 2.0 mm. It shows increasing of particle resolution has a significant impact on the evolution of free-surface. It caused the number of particle in vertical direction is increased by decreasing particle spacing, but it also will increase of computation time and total number of particles.

Table 5. Particle spacing and total particles for grid study.

Water Depth *d* (m)	Initial Particle Spacing *dp* (mm)	Total Number of Particles
0.4	2.0	5,370,127
	3.0	2,388,834
	4.0	1,351,731
	5.0	868,045
	6.0	607,864

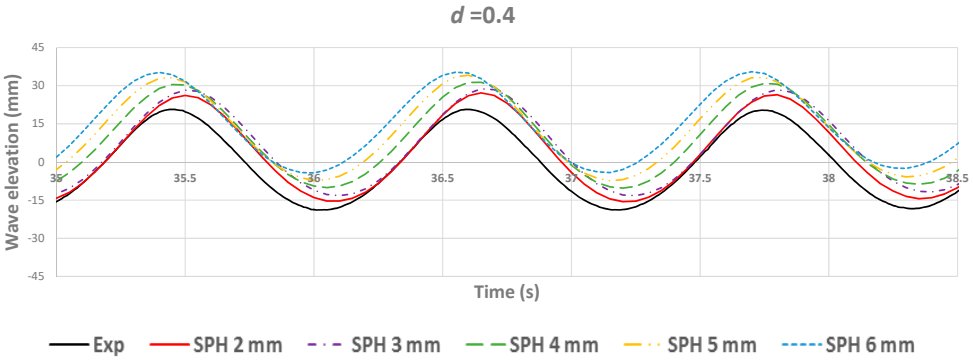

Figure 8. Grid study for T = 1.15 s, A = 16.5 mm and d = 0.4 m.

Figure 9 shows comparison results of wave elevation at 24.6 m distance from the wavemaker between the experiment and the SPH simulation for the amplitude of 50.5 mm and the period of 1.15 s of the piston motion. In all water depths, SPH shows a good agreement with the experiment in the wave amplitude from the transient state to the steady state. A certain average shift of wave elevation can be found in the SPH results as the water depth decreases. The SPH seems in good accordance with experiment. This means that the SPH simulation can reproduce the wave period and the phase velocity even in long propagation-distance. The wave surface profile is reproduced as shown in Figure 10 and it also shows that SPH has good agreement with experiment though wave profile is a non-sinusoidal shape. The quite similar result is confirmed for the cases of period 1.95 s (longer waves) as shown in Figure 11.

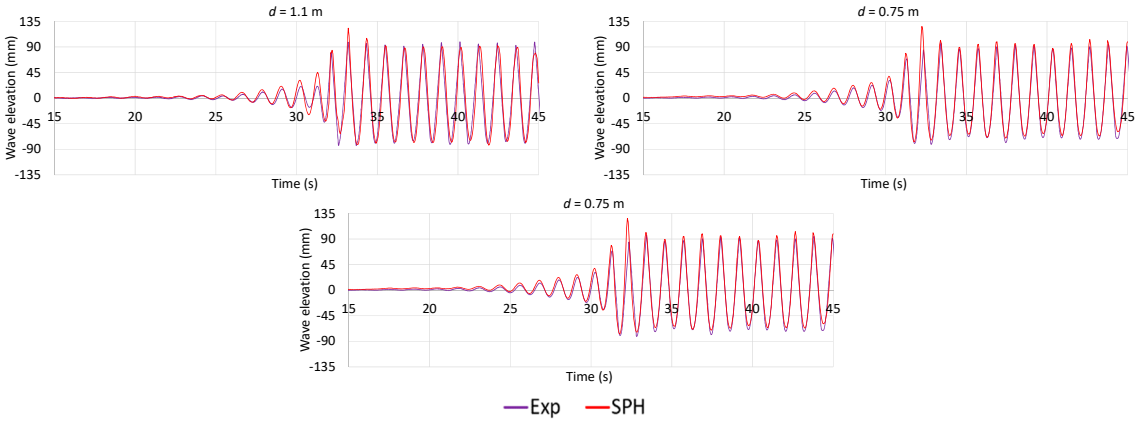

Figure 9. Comparison of wave elevation for A = 50.5 mm and T = 1.15 s with three water dept.

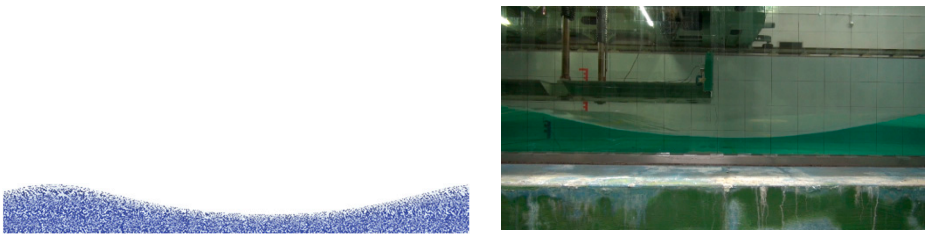

Figure 10. *Cont.*

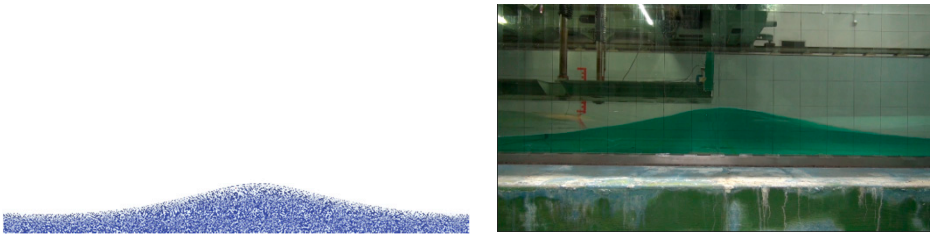

Figure 10. Comparison of wave surface profile for t = 38.2 s and 38.8 s with A = 50.5 mm, T = 1.15 s and d = 0.4 m.

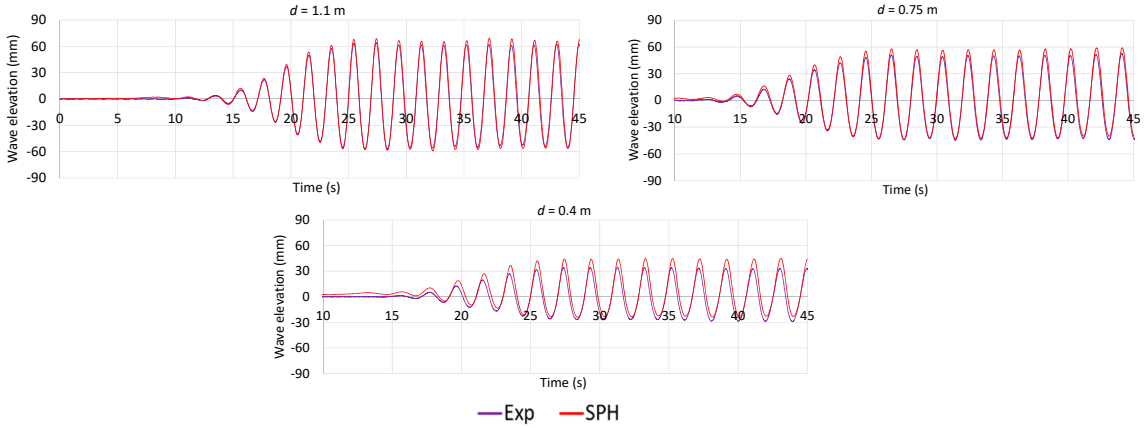

Figure 11. Comparison of wave elevation for A = 50.5 mm and T = 1.95 s with three water depths.

For further discussion on the prediction accuracy of steady wave amplitude, the SPH result is compared with the well-known Biesel transfer function proposed by Biésel and Suquet [26] as well as the experiment. The steady wave amplitude can be estimated by Equation (10) as a solution of linear theory. Where H is the height of wave and A is an amplitude of wave. Table 6 shows comparison results and SPH shows a smaller error than the Biesel transfer function in most conditions. The maximum error and the averaged error of the Biesel transfer function are 18.1% and 7.4% for T = 1.15 s, and 32% and 16% for T = 1.95 s. The Biesel transfer function becomes worse for smaller water depth in case of the shorter waves and becomes worse for larger amplitude in case of the longer waves. It's because of Biesel theory can't account for non-linear aspects that become more influential as the relative depth decrease. On the contrary, the maximum error and the averaged error of the SPH are 8.5% and 4.6% for T = 1.15 s, and 9.9% and 7.5% for T = 1.95 s this confirm that SPH can reproduce non-linear aspect caused by reduction of water depth. This result clearly demonstrates the capability of SPH for water wave problems in wide ranges of wavelength and water depth. It should be noted that the SPH simulations here are using constant parameters for all conditions. This fact might be one of the major reasons for that the SPH model is often used in civil engineering and coastal engineering in which the change of water depth cannot be neglected in many cases.

Looking at the SPH results in detail, the maximum and the second maximum errors is 9.8% found in the shallowest water depth. The experimental result shows that the wave amplitude decreases with the decrease of water depth and the increase of wave period. For example, the wave amplitude for water depth 0.4 m is about half the amplitude of water depth 1.1 m. Consequently, to this fact, the number of fluid particles in a wave height becomes smaller according to the decrease of water depth and the increase of wave period if a constant particle spacing is used. In the case of the maximum error, the number of particles in a wave height is 14. So it could be recommended to adopt at least 14 particles in a wave height to get appropriate accuracy. In some cases good representation was obtained using less than 14 particles [27,28]. In case of long distance propagation it was shown that the number of particles in vertical direction (H/dp) needs to be higher than 14. The ratio of smoothing length to particle spacing is 2.83 in case of long distance propagation: this value proved to be suitable

for the case of long distance propagation, but since this recommended value was derived from the results in a long NWT for a wide range of wave condition, it is expected to be applicable in similar conditions with the same parameters that were used in this case.

$$\frac{H}{2} = \frac{2sinh^2\left(\frac{2\pi d}{\lambda}\right)}{\frac{2\pi d}{\lambda} + sinh\left(\frac{2\pi d}{\lambda}\right)cosh\left(\frac{2\pi d}{\lambda}\right)} A \tag{10}$$

Table 6. Comparison of steady amplitude with a different method.

T (s)	A (mm)	d (m)	Exp. (mm)	SPH (mm)	SPH Error (%)	Biesel T.F. (mm)	Biesel Error (%)
1.15	16.5	1.10	32.9	30.1	8.5	32.4	1.5
		0.75	26.8	28.7	−7.1	29.5	−10.1
		0.40	20.4	19.1	6.4	19.4	4.9
	33.0	1.10	62.3	58	6.9	64.8	−4.0
		0.75	53.2	55.5	−4.3	59.0	−10.9
		0.40	40.6	39.6	2.5	38.7	4.7
	50.5	1.10	83.9	86.8	−3.5	99.1	−18.1
		0.75	81.7	81.0	0.9	90.4	−10.6
		0.40	60.6	60.0	1.0	59.3	2.1
1.95	16.5	1.10	18.2	19.6	−7.7	18.6	−2.20
		0.75	14.9	15.7	−5.4	13.0	12.8
		0.40	10.3	11.1	−7.8	7.0	32.0
	33.0	1.10	38.5	41.4	−7.5	37.3	3.10
		0.75	30.8	32.9	−6.8	26.0	15.6
		0.40	20.5	22.5	−9.8	14.0	31.7
	50.5	1.10	57.9	61.7	−6.6	57.0	1.60
		0.75	46.8	49.7	−6.2	39.8	15.0
		0.40	30.7	33.7	−9.8	21.4	30.3

SPH showed the good agreement of wave elevation but it was confirmed only for one position, i.e. 24.6 m from the wavemaker. Therefore the measurement of wave elevation was carried at three different distance, those are 10.0 m, 20.0 m and 30.0 m from the wavemaker. The comparisons of steady amplitude at three different positions are shown in Figure 12. The SPH results show good agreement not only in the wave amplitude but also in the damping rate of wave amplitude along the propagation-distance. This result suggests both the energy conservation and the energy consumption are well achieved by SPH.

Figure 12. Comparison of wave amplitude at different positions for A = 33.0 mm and d = 0.75 m.

5.2. Deformation of Wave-Surface

Next, the SPH model was applied to a problem of large deformation of wave-surface. Here the wave-surface deformation was occurred due to the sudden change of water depth by putting a box-shape obstacle as same as the experiment. The amplitude and the period of wavemaker are

50.5 mm and 1.15 s. Figure 13 shows the comparison of wave elevation at the middle position of the box-shape obstacle. Due to the so-called bank effect, wave crest was stretched in the experiment, and the SPH simulation provides a fairly similar result. In the visual comparisons of a snapshot of wave-surface deformation shown in Figure 14, the simulated wave-surface indicated by red dashed line looks quite similar with the measured wave-surface indicated by purple solid line even with the large deformation involving wave-breaking.

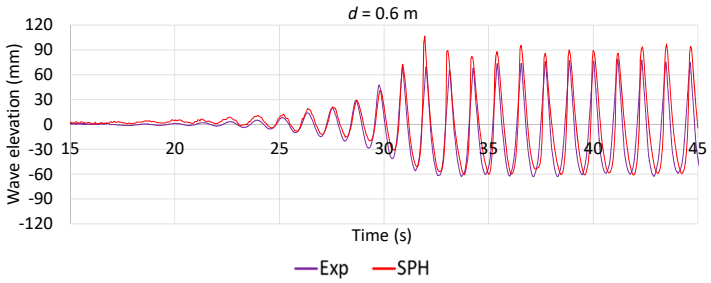

Figure 13. Comparison of wave elevation with box-shape obstacle.

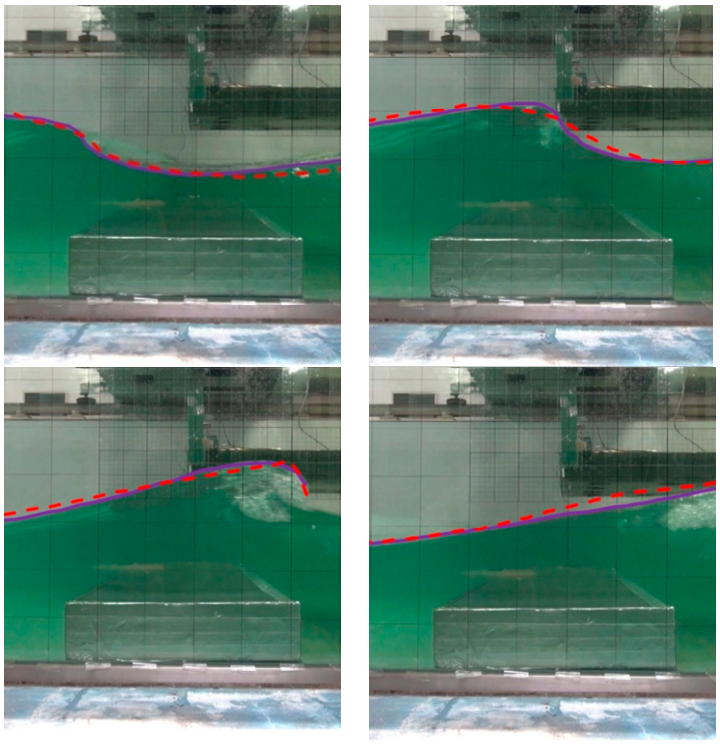

Figure 14. Visual comparison of wave-surface deformation at t = 35.0 s, 35.2 s, 35.4 s, 35.6 s.

5.3. Wave Pressure

In this subsection, the validation of SPH on the wave dynamic pressure is attempted. Before that, the hydrostatic pressure at rest condition is calculated by SPH (see Figure 15) and is compared with the analytical solution. The analytical solution of hydrostatic pressure at the bottom of the tank is 7.30 kPa and that of SPH is 7.28 kPa, so the error of SPH is only 0.9%.

Figure 16 shows the pressure variation over time calculated at several depths. Here the depth of 1.1 m means that pressure sensor is at the bottom of the tank, and the depth equal to 0 m means that the corresponding pressure sensor is at the original calm-water surface. Significant high-frequency pressure fluctuations appear at a pressure sensor located at the bottom of the tank, but these high-frequency fluctuations decrease as the detection position moves to near the free-surface. Because pressure noise is very strong in the bottom of the tank it was more favorable using pressure

sensor at the original calm-water surface. Because DualSPHysics is based on Weakly Compressible SPH (WCSPH) pressure oscillations are caused by density allowed to fluctuate while Incompressible SPH (ISPH) will give more stable result on pressure field [29–31]. Therefore the experimental result of wave pressure was converted from the bottom to the calm-water surface by multiplying cosh ($2\pi d/\lambda$) with the measured pressure, based on the linear wave theory. Figures 17 and 18 show the comparison results of wave dynamic pressure in the case of the maximum amplitude of piston motion. Note that the hydrostatic pressure is already subtracted from the measurement data, and the SPH result can be obtained only when the evaluation point is under the wave-surface. For all the investigated combinations of wave period and water depth, wave dynamic pressure predicted by SPH at free surface is acceptable as well as the wave elevation discussed before. Because the pressure sensor is located at free-surface, the negative pressure cannot capture by SPH. Further investigation of dynamic pressure at bottom of the tank is needed and will be carried out in future works. However, this paper mainly focused on the propagation of water waves for long distance, which is an essential element to be used in ocean engineering research. In case of floating bodies in a wave, for example, the contribution to the hydrodynamic force acting on the floating bodies is limited to around the free surface, and the accuracy of SPH simulation was confirmed at least near the free surface by this study.

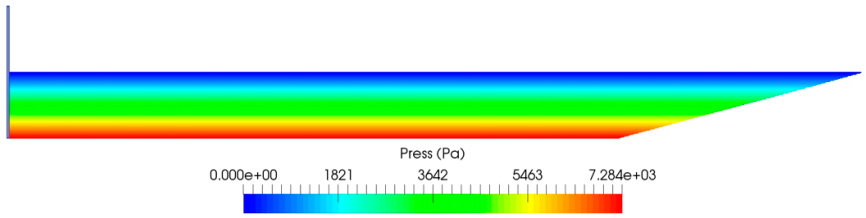

Figure 15. SPH result of hydrostatic pressure for d = 0.75 m.

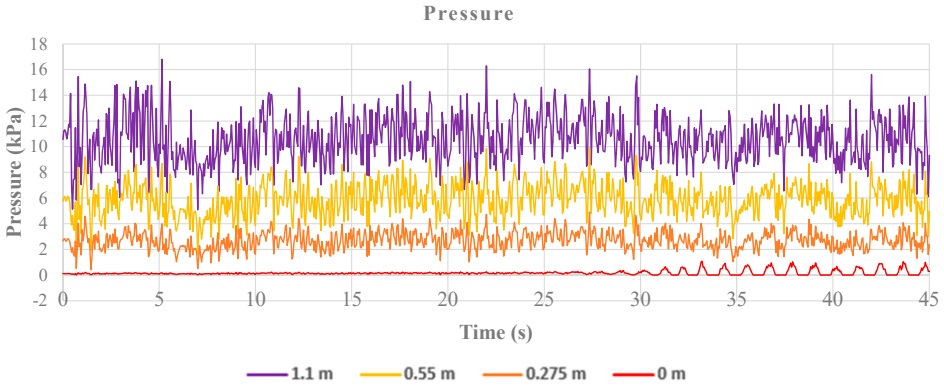

Figure 16. Pressure variation of smoothed particle hydrodynamics (SPH) at different depths with d = 1.1 and A = 50.5 mm.

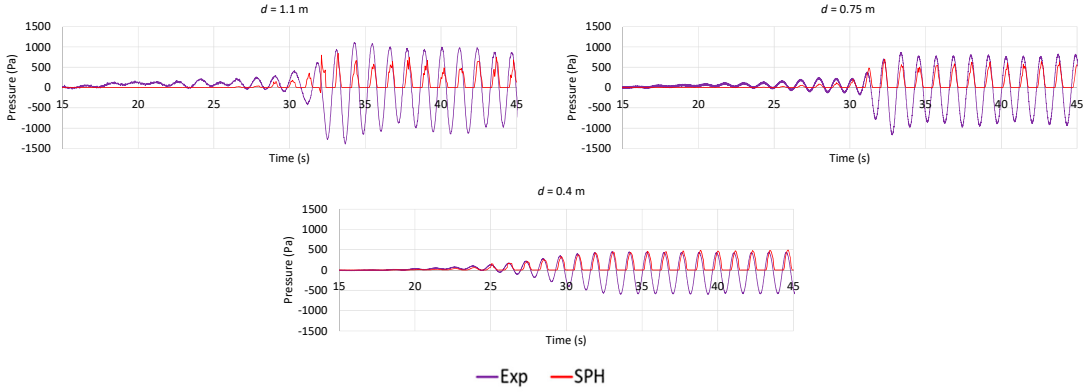

Figure 17. Dynamic wave pressure for A = 50.5 mm and T = 1.15 s.

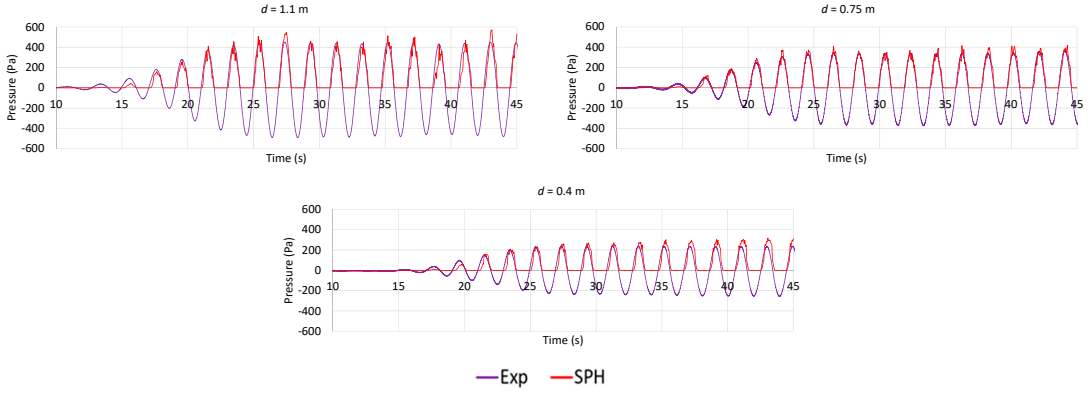

Figure 18. Dynamic wave pressure for A = 50.5 mm and T = 1.95 s.

5.4. Validation of 3-D SPH Simulation

All the discussions until here were based on the comparison results between the two-dimensional (2-D) SPH and the experiment. Since three-dimensional (3-D) simulation is sometimes required depending on problems, experimental validation of 3-D SPH is also attempted. However, it is difficult to use the same experimental data used in the 2-D SPH validation because the tremendous number of particles is required for realizing the same size of 3-D NWT. Therefore a new experiment was conducted that is suitable for the 3-D SPH validation on water waves. The experiment was conducted at the same wave basin of Kobe University and the location of the wave probe and pressure sensor was 6.0 m from the wave-maker. Regular wave trains were generated with A = 50.5 mm and T = 1.15 s for water depths of 0.4 m and 0.75 m.

The particle spacing of 3.0 mm was used in 2-D validation, so the same particle spacing is preferable to use in 3-D. However, there is a limit of an available number of particles using single GPU because of DualSPHysics ver. 4.0 has not yet implemented the parallelization using multi GPUs. For this reason, particle spacing of 4.5 mm, 1.5 times large as the 2-D case, was used for 3-D SPH simulation. In this case, the number of particles in a wave height is 28, for the water depth of 0.4 m. The dimension of NWT is shown in Figure 19. In this subsection, the 2-D NWT and the 3-D NWT have the same dimension and the width of 3-D NWT is 0.3 m. The numerical parameters for 3-D SPH are shown in Table 7. As the length of 3-D NWT is much shorter than that of 2-D NWT, a smaller value of coefh, compared to the 2-D SPH in Table 3, was used to avoid excessive computational load. The coefficient artificial viscosity, α, is also different from the 2-D SPH because its optimal value depends on other parameters, like coefh. The total number of particles for the 3-D NWT is more than 35 million for the deepest water depth, so the shallow and medium water depths, 0.4 m and 0.75 m, are only used (see Table 8). The computation time to complete 30 seconds simulation is about 2.5 weeks for the water depth of 0.75 m.

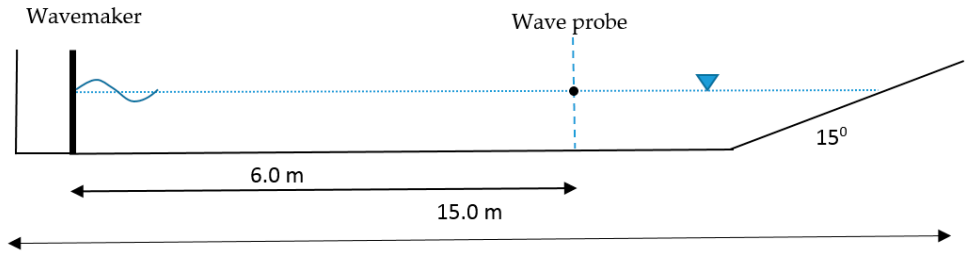

Figure 19. Schematic view of numerical wave tank for 3-D validation.

Table 7. The numerical setting in DualSPHysics (3D).

Kernel function	Wendland
Time step algorithm	Symplectic
Artificial viscosity coeff. α	0.01
Coefsound	20.0
Particle spacing (mm)	4.5
Coefh	1.2
CFL number	0.3
Delta-SPH (δ)	0.1
Simulation time (s)	30.0

Table 8. Particle spacing and the total number of particles in 3-D.

Initial Particle Spacing *dp* (mm)	Water Depth *d* (m)	Total Number of Particles
4.5	0.75	22,713,258
	0.40	12,171,792

The wave elevation of water waves 3-D SPH was compared with the experiment as well as the 2-D simulation for water depths of 0.4 m and 0.75 m, as shown in Figure 20. Here the 2-D simulation was performed using the same parameter set for the 3-D SPH, presented in Table 7, while the same particle spacing of 4.5 mm was used. The accuracies of wave elevation by 2-D and 3-D seem to be practically acceptable in term of wave elevation, but the accuracy of phase celerity by 3-D SPH becomes slightly worse 4% for the case of medium water depth with error is 6.8% for steady amplitude. This could be related to the smaller smoothing length was used for the 3-D simulation to reduce the computation time and number of particles in vertical direction are also needed to increase to get appropriate accuracy.

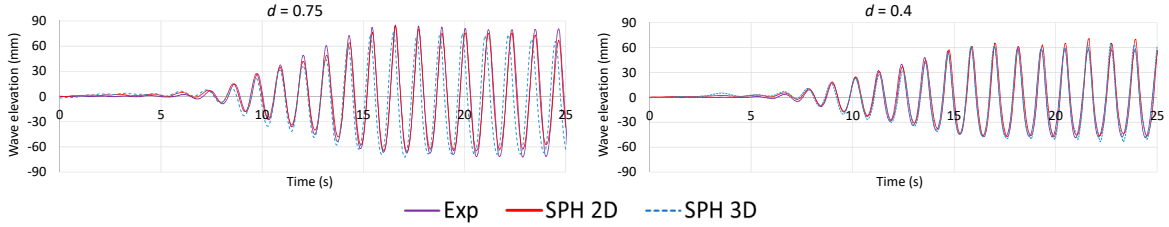

Figure 20. Comparison of wave elevation of the experiment, 2-D and 3-D SPH for A = 50.5 mm and *T* = 1.15 s.

The velocity field and velocity vector are shown in Figure 21. Using a passive wave absorber, i.e. sloped beach, reflected waves are well eliminated, so the wave elevation by the simulation can be directly compared with the experiment.

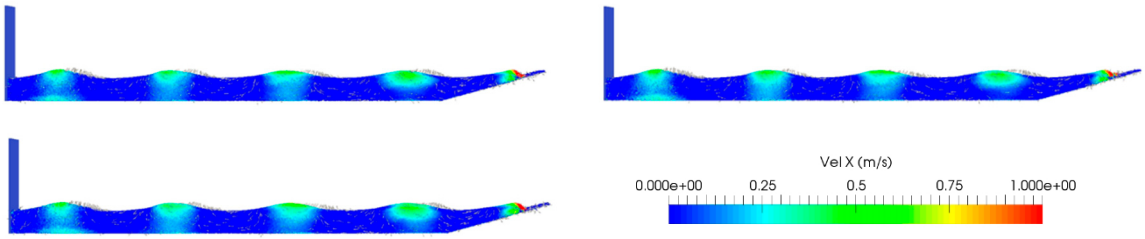

Figure 21. Velocity field and velocity vector of 3-D SPH at *t* = 17.25 s, 19.55 s & 21.85 s.

The hydrostatic pressure by 3-D SPH for water depth 0.75 m is shown in Figure 22. As same as the 2-D case, the smoothed pressure graduation can be confirmed. In this case, static pressure at the bottom of the tank is 7.17 kPa and the analytic solution is 7.30 kPa its difference 2.3%. Comparison

results of wave dynamic pressure of the experiment and the 2-D SPH and the 3-D SPH are shown in Figure 23. The good agreement of 3-D SPH and the experiment can be found for the shallow condition. The decline in accuracy is found for the middle water depth as same as the wave elevation. Because the wave dynamic pressure is validated at the height of the original calm water surface, it is easily imagined that they are closely related to each other.

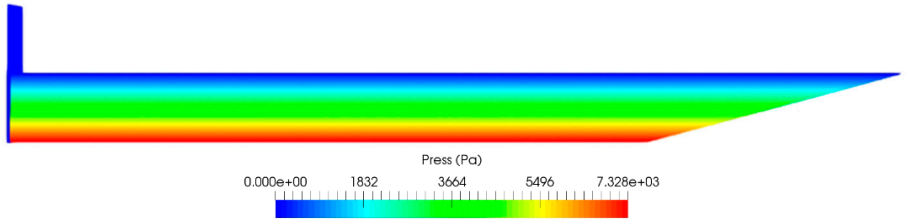

Figure 22. 3-D SPH result of hydrostatic pressure for d = 0.75 m.

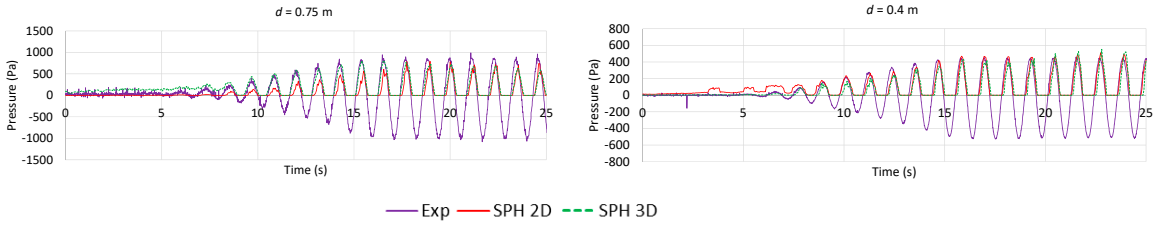

Figure 23. Comparison of wave dynamic pressure of experiment and 2-D and 3-D SPH for A = 50.5 mm and T = 1.15 s.

Since 2-D SPH was well validated for 2-D water waves in the former sections and the 3-D SPH showed comparable accuracy with 2-D SPH for the smaller NWT, it can be concluded the SPH can partly reproduce the physical character and behavior of water waves with suitable accuracy from the engineering point of view. Correct assessment of the accuracy of pressure fields requires further investigation to compare measured and calculated values at the same depth.

6. Conclusions

Systematic validation of SPH on the generation and propagation of water waves was attempted for further utilization of SPH in engineering. A dedicated experiment was conducted at a large wave basin for several water depths to obtain validation data on water waves. The 2-D simulations were executed using the numerical wave tank that has the same dimension with the real wave basin. In addition, the wave generation was executed by directly imposing the measured piston motion of wavemaker as the moving wall boundary condition. As the results of the comparison of the experiment and SPH, it is demonstrated that SPH can suitably reproduce some relevant features of the wave generation regardless of the propagation distance. Through the validation study, a recommended parameters for water wave problems was derived based on long distance propagation. In addition, the decay rate of wave amplitude along the wave tank and the large deformation of wave-surface due to the existence of obstacle were examined, and then the accuracy of SPH was satisfactory. Finally, 3-D SPH simulations of water waves were performed using a small numerical wave tank and were validated through comparisons with the experiment. As it was shown the SPH simulation can suitably reproduce, for a wide range of water depth, some characteristics of the surface profile, deformation and the celerity. In order to assess the accuracy of dynamic pressure prediction, further investigation are required.

Author Contributions: Conceptualization, H.H.; validation, A.T.; investigation, A.T.; writing—review and editing, A.T.; supervision, H.H.

Funding: This research received no external funding

Acknowledgments: The first author wishes to thank to Directorate General of Resources for Sciences, Technology and Higher Education, Ministry of Research, Technology and Higher Education of Indonesia under BPP-LN doctoral scholarship No. 181.47/E4.4/2014. This work was partially supported by JSPS KAKENHI Grant Number 17H03493.

Conflicts of Interest: The authors declare no conflict of interest

References

1. Gingold, R.A.; Monaghan, J.J. Smoothed Particle Hydrodynamics: Theory and Application to Non-Spherical Stars. *Mon. Not. R. Astron. Soc.* **1977**, *181*, 375–389. [CrossRef]
2. Lucy, L.A. Numerical Approach to the Testing of the Fission Hypothesis. *Astron. J.* **1977**, *82*, 1013–1024. [CrossRef]
3. Monaghan, J.J. Simulating Free Surface Flows with SPH. *J. Comput. Phys.* **1994**, *110*, 399–406. [CrossRef]
4. Gómez-Gesteira, M.; Cerqueiro, D.; Crespo, A.J.C.; Dalrymple, R.A. Green Water Overtopping with a SPH model. *Ocean Eng.* **2005**, *32*, 223–238. [CrossRef]
5. Le Touzé, D.; Marsh, A.; Oger, G.; Guilcher, P.M.; Khaddaj-Mallat, C.; Alessandrini, B.; Ferrant, P. SPH Simulation of Green Water and Ship Flooding Scenarios. *J. Hydrodyn. B* **2010**, *22*, 231–236. [CrossRef]
6. Colagrossi, A.; Lugni, C.; Brocchini, M.A. Study of Violent Sloshing Wave Impact Using an Improved SPH Method. *J. Hydraul. Res.* **2010**, *48*, 94–104. [CrossRef]
7. Gotoh, H.; Khayyer, A.; Ikari, H.; Arikawa, T.; Shimosako, K. On Enhancement of Incompressible SPH Method for Simulation of Violent Sloshing Flows. *Appl. Ocean Res.* **2014**, *46*, 104–115. [CrossRef]
8. Kawamura, K.; Hashimoto, H.; Matsuda, A.; Terada, D. SPH Simulation of Ship Behaviour in Severe Water-Shipping Situations. *Ocean Eng.* **2016**, *120*, 220–229. [CrossRef]
9. Hashimoto, H.; Kawamura, K.; Sueyoshi, M.A. Numerical Simulation Method for Transient Behavior of Damaged Ships Associated with Flooding. *Ocean Eng.* **2017**, *143*, 282–294. [CrossRef]
10. Violeau, D.; Rogers, B.D. Smoothed Particle Hydrodynamics (SPH) for Free Surface Flows: Past, Present and Future. *J. Hydraul. Res.* **2016**, *54*, 1–26. [CrossRef]
11. Dalrymple, R.A.; Rogers, B.D. Numerical modelling of water waves with the SPH method. *Coast. Eng.* **2006**, *53*, 141–147. [CrossRef]
12. Skillen, A.; Lind, S.; Stansby, P.K.; Rogers, B.D. Incompressible Smoothed Particle Hydrodynamics (SPH) With Reduced Temporal Noise and Generalised Fickian Smoothing Applied to Body–Water Slam and Efficient Wave–Body Interaction. *Comput. Methods Appl. Mech. Eng.* **2013**, *265*, 163–173. [CrossRef]
13. Barreiro, A.; Crespo, A.J.C.; Domínguez, J.M.; Gómez-Gesteira, M. Smoothed Particle Hydrodynamics for Coastal Engineering Problems. *Comput. Struct.* **2013**, *120*, 96–106. [CrossRef]
14. Antuono, M.; Colagrossi, A.; Marrone, S.; Lugni, C. Propagation of Gravity Waves through an SPH Scheme with Numerical Diffusive Terms. *Comput. Phys. Commun.* **2011**, *182*, 866–877. [CrossRef]
15. Altomare, C.; Dominguez, J.M.; Crespo, A.J.C.; Gonzalez-Cao, J.; Suzuki, T.; Gómez-Gesteira, M.; Troch, P. Long-Crested Wave Generation and Absorption for SPH-Based Dualsphysics Model. *Coast. Eng.* **2017**, *127*, 37–54. [CrossRef]
16. Crespo, A.J.C.; Domínguez, J.M.; Rogers, B.D.; Gómez-Gesteira, M.; Longshaw, S.; Canelas, R.; García-Feal, O. DualSPHysics: Open-Source Parallel CFD Solver Based on Smoothed Particle Hydrodynamics (SPH). *Comput. Phys. Commun.* **2015**, *187*, 204–216. [CrossRef]
17. Crespo, A.J.C.; Domínguez, J.M.; Barreiro, A.; Gómez-Gesteira, M.; Rogers, B.D. GPUs, a New Tool of Acceleration in CFD: Efficiency and Reliability on Smoothed Particle Hydrodynamics. *PLoS ONE* **2011**, *6*, e20685. [CrossRef] [PubMed]
18. Domínguez, J.M.; Crespo, A.J.C.; Valdez-Balderas, D.; Rogers, B.D. New Multi-GPU Implementation for Smoothed Particle Hydrodynamics on Heterogeneous Clusters. *Comput. Phys. Commun.* **2013**, *184*, 1848–1860. [CrossRef]
19. Violeau, D. *Fluid Mechanics and the SPH Method: Theory and Applications*; Oxford University Press: Oxford, UK, 2012.
20. Liu, G.R.; Liu, M.B. *Smoothed Particle Hydrodynamics: A Meshfree Particle Method*; World Scientific: Singapore, 2003.

21. Wendland, H. Piecewise Polynomial, Positive Definite and Compactly Supported Radial Functions of Minimal Degree. *Adv. Comput. Math.* **1995**, *4*, 389–396. [CrossRef]
22. Monaghan, J.J. Smoothed Particle Hydrodynamics. *Annu. Rev. Astron. Astrophys.* **1992**, *110*, 543–574. [CrossRef]
23. Molteni, D.; Colagrossi, A. A Simple Procedure to Improve the Pressure Evaluation in Hydrodynamic Context Using the SPH. *Comput. Phys. Commun.* **2009**, *180*, 861–872. [CrossRef]
24. Marrone, S.; Autuono, M.; Golagrossi, A.; Colicchio, G.; Le Touzé, D.; Graziani, G. δ-SPH Model for Simulating Violent Impact Flows. *Comput. Methods Appl. Mech. Eng.* **2011**, *200*, 1526–1542. [CrossRef]
25. Dean, G.A.; Dalrymple, R.A. *Water Wave Mechanics for Engineers and Scientists*; World Scientific: Singapore, 1991.
26. Biésel, F.; Suquet, F. Les Appareils Générateurs De Houle En Laboratoire-Laboratory Wave Generating Apparatus. *La Houille Blanche* **1951**, *6*, 147–165. [CrossRef]
27. Manenti, S.; Pierobon, E.; Gallati, M.; Sibilla, S.; D'Alpaos, L.; Macchi, E.; Todeschini, S. Vajont disaster: Smoothed particle hydrodynamics modeling of the Postevent 2D experiments. *J. Hydraul. Eng.* **2016**, *142*, 05015007. [CrossRef]
28. Manenti, S.; Amicarelli, A.; Todeschini, S. WCSPH with limiting viscosity for modeling landslide hazard at the slopes of artificial reservoir. *Water* **2018**, *10*, 515. [CrossRef]
29. Gu, S.; Zheng, X.; Ren, L.; Xie, H.; Huang, Y.; Wei, J.; Shao, S. SWE-SPHysics Simulation of Dam Break Flows at south-gate Gorges Reservoir. *Water* **2017**, *9*, 387. [CrossRef]
30. Zheng, X.; Ma, Q.; Shao, S.; Khayyer, A. Modelling of violent water wave propagation and impact by incompressible SPH with first-order consistent kernel interpolation scheme. *Water* **2017**, *9*, 400. [CrossRef]
31. Wang, D.; Li, S.; Arikawa, T.; Gen, H. ISPH simulation of scour behind seawall due to continuous tsunami overflow. *Coast. Eng. J.* **2016**, *58*, 1–23. [CrossRef]